DISLOCATION NUCLEATION VERSUS CLEAVAGE DECOHESION AT CRACK TIPS

Glenn E. Beltz and James R. Rice
Division of Applied Sciences
Harvard University
Cambridge, MA 02138

ABSTRACT

The competition between cleavage decohesion and dislocation emission at a crack tip is discussed here, with emphasis on a new approach to the analysis of dislocation nucleation which makes use of a Peierls-type stress versus displacement relation on a slip plane ahead of the tip. A recent analytical result by Rice shows that for a mode II or III shear crack, with a slip plane parallel to the crack plane, the criterion for nucleation is given by $G = \gamma_{us}$ (G is the energy release rate and γ_{us} is the "unstable stacking" energy associated with the sliding of atomic planes past one another). The advantage of this treatment is that it allows for the existence of an extended dislocation core during nucleation, eliminating the need for a core cutoff radius. More complicated cases involving mixed mode loadings are considered here, in which numerical solutions are required to solve for the emission criterion. It is found that tension across a slip plane slightly reduces the critical load for emission. Implications for the ductile versus brittle behavior of crystal lattices and interfaces are discussed.

Modeling the Deformation of Crystalline Solids
Edited by Terry C. Lowe, Anthony D. Rollett, Paul S. Follansbee and Glenn S. Daehn
The Minerals, Metals & Materials Society, 1991

I. INTRODUCTION

In this paper, the issue of the ductile versus brittle response of a crystal in the presence of a crack is addressed. The concept adopted here is the same as that used in later versions [1,2,3,4,5] of the Rice-Thomson model [6], in which the competition between cleavage decohesion and dislocation emission is quantified via the parameters G_{cleave}, the energy release rate for cleavage, and G_{disl}, the energy release rate associated with the emission of a single dislocation on a slip plane emanating from the crack tip. In fig. 1, the basic premise of the model is illustrated. If $G_{cleave} < G_{disl}$, then the crack propagates in a brittle manner; conversely, if $G_{disl} < G_{cleave}$, then a dislocation moves away from the crack tip thus blunting and "shielding" the crack tip from further increases in applied loading. Dislocation emission from crack tips has been directly observed by use of the etch pit technique [7], x-ray topography [8], and in-situ TEM observations [9,10].

The primary purpose of this paper is to incorporate a new approach to analyzing dislocation nucleation. Previous models for calculating G_{disl} were based on elasticity theory for complete dislocations, and required a knowledge of the core cutoff radius r_c and the core energy E_{core} [1,6,11]. Argon [12] and, more recently, Schoeck [13] have recognized that a full dislocation is likely to emerge unstably from an incomplete, incipient dislocation at the tip, but a reasonably exact treatment of the phenomenon has been given only recently [14]. That treatment, discussed here, solves the elasticity problem of a traction-free crack with a Peierls-type stress versus displacement relation being satisfied as a boundary condition along a slip plane ahead of the crack tip. Once this interfacial constitutive relation is specified, and the elasticity problem solved, there is no need for core cut-off parameters. The advantage of this method is that it allows for the existence of an extended dislocation core during nucleation, and eliminates uncertainty involved with choosing the core parameters.

Several theoretical and experimental studies have revealed that the mechanical behaviour of a grain boundary (or any bimaterial interface) is strongly dependent on the orientation of the joined crystal(s) (see [3] and references therein). Another effect is the type of loading (i.e., the relative amounts of applied mode I, II, and III stress intensity factors). These effects are closely related because they control dislocation emission through their determination of the resolved shear stress and tensile stress on slip planes ahead of a crack tip. In the current work, the specific problem of the emission of an edge dislocation on a slip plane which is coplanar with the crack plane is analyzed (see fig. 2). Emission criteria are developed for combined mode I and mode II loading.

II. DECOHESION AT A CRACK TIP

The Griffith criterion for crack growth in the absence of plasticity may be used to estimate the energy release rate for cleavage (e.g., [4,15]),

$$G_{cleave} = 2\gamma_s, \tag{1}$$

where $2\gamma_s$ is twice the surface energy, and corresponds to the reversible work of fracture. For interfacial fracture, $2\gamma_s$ generalizes to $2\gamma_{int}$, and is given by

$$2\gamma_{int} = \gamma_s^A + \gamma_s^B - \gamma_b^{A/B}. \quad (2)$$

The parameters γ_s^A, γ_s^B, and $\gamma_b^{A/B}$ correspond to the surface free energies of materials A and B, and the interfacial free energy prior to separation.

A more sophisticated treatment of decohesion is given by the cohesive zone model, which attempts to take into account the non-uniform decohesion that occurs as a crack propagates. In this model, two joined elastic media are initially in contact and decohere within a "transition" zone. A stress versus separation relation $\sigma = \sigma(\delta)$ is assumed to apply along the decohering interface. Application of a well-known J-integral calculation gives [16,17]

$$G_{cleave} = \int_0^\infty \sigma(\delta)d\delta = 2\gamma_{int} \quad (3)$$

in cases when the decohesion zone is much smaller than the overall crack length [4,16]. Note that this is the same result predicted by the Griffith model.

Effects relating to lattice discreteness have been suggested as one reason why $2\gamma_s$ seems to be a lower bound on G_{cleave}. The phenomenon of "lattice trapping" is the excess of G_{cleave} over $2\gamma_s$, where G_{cleave} has been calculated for an ideally brittle crystal via one of the well-known atomic simulation procedures [18,19]. This difference may exist even if the interaction potentials used in the calculation are consistent with the uniform, brittle decohesion of bonds on the fracture path. Another effect on G_{cleave} is the coupling that may occur between x, y, and z relative displacements (denoted δ_x, δ_y, and δ_z) on the cleavage plane. The J-integral argument in connection with eq. (3) generalizes to

$$G_{cleave} = J_{cleave} = \int_{(0,0,0)}^{(\delta_x,\delta_y,\delta_z)^{tip}} \sigma_{y\alpha}(\delta_x,\delta_y,\delta_z)d\delta_\alpha = \Phi(\delta_x^{tip},\delta_y^{tip},\delta_z^{tip}), \quad (4)$$

where $\Phi(\delta_x, \delta_y, \delta_z)$ is the potential across the cleavage plane and thus $\sigma_{y\alpha} = \partial\Phi / \partial\delta_\alpha$ (α=x, y, z with summation over repeated indices). For large δ_y^{tip}, Φ is independent of δ_x and δ_z, and equal to $2\gamma_s$. Nevertheless, eq. (4) doesn't preclude the possibility that δ_x and δ_z may lead to local maxima of G for $G < G_{cleave}$, possibly corresponding to dislocation nucleation, and thus (by shielding effects) causing the macroscale, "applied" G to significantly exceed G_{cleave}. These displacement components may be brought on by shear loading in the vicinity of the crack tip, or by effects relating to dissimilarity in elastic properties if bimaterial fracture is under consideration.

III. DISLOCATION NUCLEATION AT A CRACK TIP

Previous versions of the Rice-Thompson model have treated dislocation nucleation by two methods. Both proceed by assuming the existence of a freshly generated dislocation at a relatively small distance (turning out to be less than a few atomic spacings) away from the crack tip, on a slip plane which intersects the crack front. A drawback of both, as well as the new method to be discussed in this paper, is that the analysis may be straightforwardly applied

only to cases in which the slip plane(s) intersect the crack front. Following [1], however, we may imagine a scenario in which dislocations are emitted when a moving crack front undergoes local deviations which bring it into line with a potentially active slip plane.

The first method assumes the dislocation line is straight (see fig. 3). Using an elasticity solution for the dislocation in the presence of a crack tip the force on the dislocation can be determined as a function of distance from the tip and the applied stress intensity factor(s). For a mode I loading, the force is [6]

$$f = -\frac{\mu b^2}{4\pi r}\left[\frac{\cos^2\phi}{1-\nu} + \sin^2\phi\right] + \frac{SbK_I}{\sqrt{r}}, \tag{5}$$

where r is distance from the tip, b is the length of the Burgers vector, ϕ is the orientation of the Burgers vector in the slip plane, and $S = S(\theta)$ is a geometric factor such that $SK_I/\sqrt{r}$ is the resolved shear stress on the slip plane. Emission of the dislocation is assumed to occur when K_I is large enough to make f vanish when the position r is equal to one core radius away from the tip, i.e., setting eq. (5) equal to zero for $r = r_c$ gives the emission criterion. This procedure insures that the Peach-Koehler force on the dislocation is larger than the image force tending to draw the dislocation back into the tip for all $r > r_c$. One drawback to this formulation is that the core radius is an uncertain parameter [20]; in fact, the entire concept of a "core" radius loses its meaning while a dislocation is nucleated.

A second method presupposes the existence of a dislocation loop ahead of the crack tip (see fig. 4). The energy of this configuration may be calculated; it is the sum of contributions from the self energy of the half-loop, the core energy, and the surface energy of the ledge created at the crack tip, less the work done by applied loads to expand the loop to a given radius. For the simple case of mode I loading, the energy is given by [2,3,6,11]

$$E = \pi r\left[\alpha b^2 \ln\left(\frac{8mr}{e^2 b}\right) + E_{core}\right] + 2rE_{ledge} - 3.5br^{3/2}SK_I, \tag{6}$$

where $\alpha = (2-\nu)\mu/8\pi(1-\nu)$ is the prelogarithmic energy factor and is roughly 10% of the shear modulus, and m is a constant of order 1-2 [21]. The critical stress intensity factor for emission and radius r at instability are found by [1,2]

$$\frac{\partial E}{\partial r} = 0 \tag{7a}$$

$$\frac{\partial^2 E}{\partial r^2} = 0. \tag{7b}$$

The derivatives are at fixed K_I; the first condition characterizes equilibrium states (r and K_I pairs) and the second the K_I value at which the energy ceases to be a minimum at a given state (transition from $\partial^2 E/\partial r^2 > 0$ at lower K_I to $\partial^2 E/\partial r^2 < 0$ at higher K_I). The solution for r is, however, typically of the order b, whereas equations such as (6) are relatively unambiguous only for $r >> b$.

Early versions of these models attempted to show the effect of slip plane orientation and

only to cases in which the slip plane(s) intersect the crack front. Following [1], however, we may imagine a scenario in which dislocations are emitted when a moving crack front undergoes local deviations which bring it into line with a potentially active slip plane.

The first method assumes the dislocation line is straight (see fig. 3). Using an elasticity solution for the dislocation in the presence of a crack tip the force on the dislocation can be determined as a function of distance from the tip and the applied stress intensity factor(s). For a mode I loading, the force is [6]

$$f = -\frac{\mu b^2}{4\pi r}\left[\frac{\cos^2\phi}{1-\nu} + \sin^2\phi\right] + \frac{SbK_I}{\sqrt{r}}, \tag{5}$$

where r is distance from the tip, b is the length of the Burgers vector, ϕ is the orientation of the Burgers vector in the slip plane, and $S = S(\theta)$ is a geometric factor such that $SK_I / \sqrt{r}$ is the resolved shear stress on the slip plane. Emission of the dislocation is assumed to occur when K_I is large enough to make f vanish when the position r is equal to one core radius away from the tip, i.e., setting eq. (5) equal to zero for $r = r_c$ gives the emission criterion. This procedure insures that the Peach-Koehler force on the dislocation is larger than the image force tending to draw the dislocation back into the tip for all $r > r_c$. One drawback to this formulation is that the core radius is an uncertain parameter [20]; in fact, the entire concept of a "core" radius loses its meaning while a dislocation is nucleated.

A second method presupposes the existence of a dislocation loop ahead of the crack tip (see fig. 4). The energy of this configuration may be calculated; it is the sum of contributions from the self energy of the half-loop, the core energy, and the surface energy of the ledge created at the crack tip, less the work done by applied loads to expand the loop to a given radius. For the simple case of mode I loading, the energy is given by [2,3,6,11]

$$E = \pi r\left[\alpha b^2 \ln\left(\frac{8mr}{e^2 b}\right) + E_{core}\right] + 2rE_{ledge} - 3.5br^{3/2}SK_I, \tag{6}$$

where $\alpha = (2-\nu)\mu / 8\pi(1-\nu)$ is the prelogarithmic energy factor and is roughly 10% of the shear modulus, and m is a constant of order 1-2 [21]. The critical stress intensity factor for emission and radius r at instability are found by [1,2]

$$\frac{\partial E}{\partial r} = 0 \tag{7a}$$

$$\frac{\partial^2 E}{\partial r^2} = 0. \tag{7b}$$

The derivatives are at fixed K_I; the first condition characterizes equilibrium states (r and K_I pairs) and the second the K_I value at which the energy ceases to be a minimum at a given state (transition from $\partial^2 E / \partial r^2 > 0$ at lower K_I to $\partial^2 E / \partial r^2 < 0$ at higher K_I). The solution for r is, however, typically of the order b, whereas equations such as (6) are relatively unambiguous only for $r >> b$.

Early versions of these models attempted to show the effect of slip plane orientation and

combined K_I, K_{II}, K_{III} loading modes on dislocation emission, and to extend the formulation to an interface with segregated solute atoms. The greatest effect of impurity atoms seems to be on G_{cleave} through a lowering of $2\gamma_{int}$ (for "normal" segregators) [15]. Dislocation emission may also be affected, however, through a possible solute pinning effect [22], and there is also a possibility that some segregants, initially on a crack-containing interface, could segregate along the core of an emerging dislocation and affect emission (as discussed in connection with hydrogen by Anderson, Wang, and Rice [23]). The emission of dislocations in dissociated form has been treated extensively in [2,11].

To summarize the new approach [14], assume now the existence of a Peierls-type shear stress τ ($\equiv \sigma_{yx}$) versus relative atomic displacement (denoted Δ_x) relation such as the sinusoidal representation in fig. 5; Δ_x denotes the shift of one atomic plane relative to another at the slip surface. This curve gives the shear stress needed to locally shear atoms with respect to one another on a given slip plane, and is the fundamental input to the Peierls-Nabarro dislocation model [24,25]. The initial slope of such a curve corresponds with an appropriate shear modulus. The parameter b is the length of a Burgers vector and represents the periodicity of the stress-displacement relation. This type of data has been calculated through the use of pair potentials or the embedded atom method by several researchers [26,27,28]. The integral of such a curve from $\Delta_x = 0$ to the unstable equilibrium position at which the shear stress next vanishes (at $\Delta_x = b/2$ in simple cases) has been called [14] the *unstable stacking energy*, denoted γ_{us}; the role of this parameter in the dislocation nucleation process will be discussed shortly.

Consider a semi-infinite crack subject to mode II loading, in which this Peierls-type stress versus displacement relation is taken to be the constitutive relation on a slip plane which is coplanar with the crack (see fig. 2). With the exception of the slip plane, the material is here taken as an isotropic, linear elastic solid with shear modulus μ and Poisson's ratio ν; some results, like eqs. (10) and (11) to follow, do not require those assumptions [14]. Define δ_x as the displacement discontinuity on a mathematical cut coincident with the slip plane. We relate δ_x to the displacement Δ_x of the atomic planes at $y = \pm h/2$ by

$$\delta_x = u_x^{(+)} - u_x^{(-)} = \Delta_x - \frac{\tau h}{\mu}, \tag{8}$$

where h is the interplanar spacing. This idealized cut represents the slip plane, and by adding to the displacement discontinuity δ_x across the cut (in what is otherwise considered a linear elastic continuum) the additional "elastic" displacement $h\tau/\mu$, we simulate approximately the relative displacement $\Delta_x = \delta_x + h\tau/\mu$ between atomic planes a distance h apart. If τ is now plotted versus δ_x, the curve becomes skewed so as to give an infinite slope at the origin (see fig. 6). The integral of τ over half of a cycle remains equal to γ_{us}, however.

In the following calculation, the J-integral [17] is used to predict an emission criterion for the situation just discussed, in a manner closely related to its application to tensile decohesion summarized in connection with eq. (3). Within this framework, an "incipient dislocation" exists if the function $\delta_x(x)$ is nonzero as distance x approaches zero. Evaluation of the J integral on the path Γ_{far} in fig. 7 gives

$$J = \frac{1-\nu}{2\mu} K_{II}^2 = G \tag{9}$$

when the slit length is much smaller than the crack length (or any other overall length scale associated with the crack-containing elastic body). The quantity G is the energy release rate that would ensue if the crack were to move as a classical singular crack (without a shear or decohesion zone at its tip) quasi-statically under the given level of K_{II}.

Evaluation of the J-integral on the path Γ_{slit} (see fig. 7) gives

$$J = -\int_0^{R_0} \tau \frac{\partial \delta_x}{\partial x} dx = \int_0^{\delta_{tip}} \tau(\delta_x) d\delta_x, \tag{10}$$

where it is assumed that $\delta_x(x)$ has decayed effectively to zero for some sufficiently large distance R_0 (typically, of order 5b). The parameter δ_{tip} is the displacement evaluated at x = 0.

If a τ versus δ_x curve of the form shown in fig. 6 is assumed, then a plot of J versus δ_{tip} would rise monotonically until $\delta_{tip} = b/2$, then J would decrease giving instability to the atomic configuration. The dislocation nucleation criteria is therefore

$$J_{disl} = \int_0^{b/2} \tau(\delta_x) d\delta_x \equiv \gamma_{us}. \tag{11}$$

More generally, the integral extends to the first value of $\delta_x > 0$ at which energy $\Phi = \int \tau d\delta_x$ has a maximum. Thus, $G = \gamma_{us}$ is the condition for nucleation of a pure edge dislocation , on a slip plane ahead of the crack tip and parallel to the crack plane; the corresponding K_{II} is, from (9) and (11),

$$K_{II}^{disl} = \sqrt{\left(\frac{2\mu}{1-\nu}\right)\gamma_{us}}. \tag{12}$$

The derivation for a screw dislocation under a mode III loading proceeds similarly, again with the result $G = \gamma_{us}$ and, because $G = K_{III}^2 / 2\mu$,

$$K_{III}^{disl} = \sqrt{2\mu\gamma_{us}}. \tag{13}$$

Complications arise, however, when we include in the model the effects of normal tractions and dilatant opening across the slip plane. This situation occurs if some mode I loading is added to the mode II situation just discussed, or in more realistic cases when the slip plane is inclined with respect to the crack plane. There is no reason to assume that a given τ versus δ_x curve retains its shape if tension is superposed; hence the effect of superposed tension on the "effective" γ_{us} must be investigated.

Although the current work is for the simplified case when the slip and cleavage planes are coplanar, cases involving inclined slip planes may be modelled (approximately) by

considering the "effective" K_{II} and K_{III} based on shear stresses of the elastic singular field along the slip plane. For example, the emission criterion for an edge dislocation on an inclined slip plane under a mode I loading may be determined by replacing the left side of eq. (12) by $\sqrt{2\pi}S(\theta)K_I$, where S is as defined in connection with eq. (5). This procedure neglects any effect of tensile stresses across the slip plane; that can be treated in a similar approximate manner by defining also an effective K_I, based on tensile stress along the inclined slip plane, and using such results as we give in the next section, for nucleation under mixed mode loading. Work is in progress, however, to give a more reasonably exact treatment of emission on inclined planes.

IV. GENERAL LOADING OF A SLIP PLANE IN THE PRESENCE OF A CRACK

A. Combined Tension and Shear Relations

Let Δ_y be the relative atomic separation across the slip plane (see fig. 8). Analogous to the case for shearing, a suitable displacement variable for the mathematical cut representing the slip plane may be defined:

$$\delta_y = u_y^{(+)} - u_y^{(-)} = \Delta_y - \frac{L^2\sigma}{2\gamma_s}. \tag{14}$$

The quantity $2\gamma_s/L$ is an effective Young's modulus for tension across the slip plane and corresponds to the initial slope of the σ ($\equiv \sigma_{yy}$) versus Δ_y relation to be discussed shortly [15]. Here a particular form of the τ versus Δ_x and σ versus Δ_y relations are chosen for the purpose of solving some particular problems. Assume that the curve in fig. 5 is a sinusoid

$$\tau = \frac{\pi\gamma_{us}}{b}\sin\left(\frac{2\pi\Delta_x}{b}\right), \tag{15}$$

where the amplitude factor is chosen such that

$$\int_0^{b/2}\tau(\Delta_x)d\Delta_x = \gamma_{us}. \tag{16}$$

Take this to be the proper form for τ when Δ_y is zero. The corresponding relation for tensile decohesion is taken to be

$$\sigma = \frac{2\gamma_s}{L^2}\Delta_y e^{-\Delta_y/L} \tag{17}$$

when $\Delta_x = 0$. This is an example of a stress versus separation relation as discussed in section II, and follows from the well-known fit, with energy proportional to $-(L+\Delta_y)\exp(-\Delta_y/L)$, to the universal bonding correlation of Rose, et. al. [29,30,31]. The parameter L has been suggested as scaling with the Thomas-Fermi screening length; here it can be loosely interpreted as the characteristic length associated with the decohesion process (σ reaches its maximum, at $\Delta_x = 0$, when $\Delta_y = L$). The constants in front are chosen to enforce

$$\int_0^\infty \sigma(\Delta_y)d\Delta_y = 2\gamma_s, \tag{18}$$

as required by the definition of $2\gamma_s$.

For general loadings the functions $\tau(\Delta_x,\Delta_y)$ and $\sigma(\Delta_x,\Delta_y)$ must be derivable from a potential function which corresponds to the energy per unit area on the slip plane via the relations

$$\tau = \frac{\partial \Psi}{\partial \Delta_x} \tag{19a}$$

$$\sigma = \frac{\partial \Psi}{\partial \Delta_y}, \tag{19b}$$

which are equivalent to the requirement

$$\frac{\partial \sigma}{\partial \Delta_x} = \frac{\partial \tau}{\partial \Delta_y}. \tag{20}$$

The potential Ψ is related to the potential Φ of equation (4) by $\Psi = \Phi + \tau^2 h / 2\mu + L^2\sigma^2 / 4\gamma_s$, which follows from equations (8) and (14), and from $\sigma_{y\alpha} = \partial\Psi / \partial\Delta_\alpha = \partial\Phi / \partial\delta_\alpha$.

We now proceed by assuming the following generalized forms for $\tau(\Delta_x,\Delta_y)$ and $\sigma(\Delta_x,\Delta_y)$ involving functions $A(\Delta_y)$, $B(\Delta_x)$, and $C(\Delta_x)$ to be determined:

$$\tau = A(\Delta_y)\sin\left(\frac{2\pi\Delta_x}{b}\right) \tag{21a}$$

$$\sigma = \left[B(\Delta_x)\Delta_y - C(\Delta_x)\right]e^{-\Delta_y/L}. \tag{21b}$$

Enforcing eqs.(16), (18), and (20) with $C(0) = 0$, and requiring that τ and σ vanish as $\Delta_y \to \infty$, leads to the following as the most general possible expressions for A, B, and C:

$$A(\Delta_y) = \frac{\pi\gamma_{us}}{b} - \frac{2\pi\gamma_s}{b}\left\{q\left(1 - e^{-\Delta_y/L}\right) - \left(\frac{q-r}{1-r}\right)\frac{\Delta_y}{L}e^{-\Delta_y/L}\right\} \tag{22a}$$

$$B(\Delta_x) = \frac{2\gamma_s}{L^2}\left\{1 - \left(\frac{q-r}{1-r}\right)\sin^2\left(\frac{\pi\Delta_x}{b}\right)\right\} \tag{22b}$$

$$C(\Delta_x) = \frac{2\gamma_s}{L}\frac{r(1-q)}{1-r}\sin^2\left(\frac{\pi\Delta_x}{b}\right), \tag{22c}$$

where

$$q = \frac{\gamma_{us}}{2\gamma_s}, \quad r = \frac{\Delta_y^*}{L}, \tag{23}$$

and where Δ_y^* is the value of Δ_y after shearing to the state $\Delta_x = b/2$ under conditions of zero tension, $\sigma = 0$ (i.e., relaxed shearing). The parameter r is referred to here as the "dilation parameter." It is possible to obtain an explicit form for Ψ by combining eqs. (21) and (22) and then integrating; in fact, when $q = r$, it is the same form used by Needleman [32] in conjunction with the analysis of the decohesion of a viscoplastic block from a rigid substrate. The embedded atom method has been successfully employed to estimate L/b, q, and r; the results of one such study [28] are used as a guideline for estimating the parameters used in this investigation. Recent estimates suggest that q ranges from 0.05 to 0.07 in fcc materials, assuming a dislocation is emitted as a pair of partials [28]. Estimates for bcc materials, based on results in [26] and [33], show that q is about 0.12 for iron and may be as large as 0.3 for others.

B. Solutions for Combined Shear and Tensile Loading

Consider again a semi-infinite crack in an infinite elastic medium, and a slip plane which is modelled as a mathematical slit (of length R_0) which obeys the constitutive relations developed in the previous section (see fig. 9). Rigorously, this slit should be semi-infinite; in practice, however, the nonlinearities in the constitutive relations effectively disappear (i.e., the δ_α are effectively zero) beyond a finite distance from the crack tip, so R_0 may be regarded as finite for later numerical solutions. Let x denote the distance from the actual crack tip, and ξ denote the distance *backwards* from the end of the slit. We proceed by treating this situation as if the crack terminates at $\xi = 0$. The faces of the "crack" are loaded by the tractions $\tau[\delta_x(\xi),\delta_y(\xi)]$ and $\sigma[\delta_x(\xi),\delta_y(\xi)]$ immediately behind the tip, i.e. in the range $0 < \xi < R_0$. Using the elastic solution for the displacements which result from applying a point load a finite distance behind a crack tip [34], two coupled integral equations may be written:

$$\delta_x(\xi) = \frac{4K_{II}(1-\nu)}{\mu}\sqrt{\frac{\xi}{2\pi}} - \int_0^{R_0} \tilde{D}(\xi,\xi')\tau(\delta_x,\delta_y)d\xi' \tag{24a}$$

$$\delta_y(\xi) = \frac{4K_{I}(1-\nu)}{\mu}\sqrt{\frac{\xi}{2\pi}} - \int_0^{R_0} \tilde{D}(\xi,\xi')\sigma(\delta_x,\delta_y)d\xi'. \tag{24b}$$

The kernel is given by

$$\tilde{D}(\xi,\xi') = \frac{4(1-\nu)}{\mu\pi}\begin{cases} \tanh^{-1}\sqrt{\frac{\xi}{\xi'}} & 0 < \xi < \xi' \\ \coth^{-1}\sqrt{\frac{\xi}{\xi'}} & \xi' < \xi < R_0, \end{cases} \tag{25}$$

where ξ is the point where the displacement is evaluated and ξ' is the position of the point load. The first term on the right in each integral equation represent the displacements that would occur on the crack faces due to the applied K_I and K_{II} if the crack face on $0 < \xi < R_0$ were

traction free.

Since the functions $\delta_\alpha(\xi)$ are expected to be nontrivial for ξ near R_0, the calculations are carried out in a reference frame centered at the actual crack tip; changing variables such that eqs. (24a) and (24b) are expressed in terms of x gives

$$\delta_x(x) = \sqrt{\frac{16G(1-\nu)(R_0-x)}{\mu\pi}}\sin\psi - \int_0^{R_0} D(x,x')\tau(\delta_x,\delta_y)dx' \tag{26a}$$

$$\delta_y(x) = \sqrt{\frac{16G(1-\nu)(R_0-x)}{\mu\pi}}\cos\psi - \int_0^{R_0} D(x,x')\sigma(\delta_x,\delta_y)dx' \tag{26b}$$

with the newly defined kernel

$$D(x,x') = \frac{4(1-\nu)}{\mu\pi}\begin{cases} \tanh^{-1}\sqrt{\dfrac{x-R_0}{x'-R_0}} & x' < x < R_0 \\ \coth^{-1}\sqrt{\dfrac{x-R_0}{x'-R_0}} & 0 < x < x'. \end{cases} \tag{27}$$

Note that eqs. (26a) and (26b) are expressed in terms of G and ψ rather than K_I and K_{II}. The parameter ψ is the phase angle of the applied load, and is defined by $\tan\psi = K_{II}/K_I$. Eqs. (26a) and (26b) are solved for various values of ψ between 0° and 90°, corresponding to loading situations ranging from pure tension to pure shear. The parameters L/b and q are taken to be 0.2 and 0.4, respectively. The dilation constant r is taken to be 0 and 0.2. The parameter q borders on the range of our predictions for some of the harder bcc materials, such as chromium, molybdenum, or tungsten; however, no attempt is made here to characterize any particular material. Furthermore, the interplanar spacing h is taken to be equal to the Burgers vector b.

The solution method proceeds by discretizing the region $0 < x < R_0$ into sixty elements. The elements are chosen to vary in size along the domain so as to give a finer "mesh" near the actual crack tip; the nodal points are given by the relation

$$x_k = R_0\left[1-\cos\left\{\frac{\pi(k-1)}{120}\right\}\right], \tag{28}$$

where $k = 1,\ldots 60$. The unknown functions $\delta_x(x)$ and $\delta_y(x)$ are then characterized each by a vector with 60 components. Equations (26a) and (26b) are thus transformed into the following set of nonlinear algebraic equations

$$0 = -\delta_x^k + L_k\sin\psi - \left(\int_0^{R_0} D_k(x')Q_j(x')dx'\right)T_j \tag{29a}$$

$$0 = -\delta_y^k + L_k\cos\psi - \left(\int_0^{R_0} D_k(x')Q_j(x')dx'\right)S_j, \tag{29b}$$

where Q_j is a suitable set of interpolation functions, $D_k(x') = D(x_k,x')$, etc.

Eqs. (29a) and (29b) are solved by choosing a low value of G, and iterating to convergence with the Newton-Raphson method. In most cases, convergence is obtained after only two or three iterations. The applied G is then incremented, and the procedure is repeated using the previous solution as the initial guess. As solutions are obtained for increasing G, the determinant of the Jacobian matrix det J of eqs. (29a,b) is monitored. In all cases observed, this parameter rapidly decreases towards zero in a narrow range of G (see figs. 10 and 11 for examples). When this determinant is zero, eqs. (29a,b) are singular and therefore no solution is possible. The sharp decrease in det J is interpreted here as the onset of instability, and the solution procedure is halted.

V. RESULTS AND DISCUSSION

In fig. 12, displacement profiles are shown for pure shear ($\psi = 90°$) and $r = 0$ at various load levels up to instability. The characteristic length over which δ_x is appreciable is roughly $(2-3)b$. This length gives a measure of the "half-width" of the incipient edge dislocation that exists at the crack tip. If the Peierls-Nabarro dislocation model is applied to a single edge dislocation (not in the presence of a crack tip) the half-width is given by h/2(1-v), where h is the interplanar spacing [35]. This quantity is arbitrarily defined as the distance over which $b/4 < \delta_x < b/2$, and is equal to about 0.75b for the isolated dislocation (assuming $b = h$, to be consistent with the way the equations are set up in this study). Applying the same definition to the incipient dislocation gives a width of about 2b. The fact that the dislocation core seems to be wider prior to emission adds more uncertainty to the Rice-Thomson equations for nucleation, which use a core cut-off concept. The greater width also makes use of the Peierls concept yet more applicable for dislocation nucleation from a crack tip than it is for a dislocation in an otherwise perfect crystal.

At instability, the shear displacement at the crack tip is b/2, and the applied G is only slightly larger than γ_{us}, thus there is close agreement with the exact result for this simple mode II case as outlined in section III; the very small difference is due to the numerical procedure. In fig. 13, the applied G is plotted versus the shear displacement at the tip. As expected, the curve is locally flat at $\delta_x^{tip} = b/2$, indicating a local maximum in G.

The opposite limiting case of pure tension ($\psi = 0°$) is depicted in the next series of figures. Fig. 14 shows the opening profiles at various load levels up to instability. Since $\Delta_x = 0$ everywhere, the parameter r is irrelevant. Fig. 15 shows the variation of the applied G with δ_y^{tip}. The curves level off at $G = 2\gamma_s$, thus giving agreement with the theory of the cohesive zone model. The half-width of a profile here is synonymous with the "transition zone" discussed in connection with the cohesive zone model, and is of comparable magnitude to that estimated in [15].

The results for general combined tensile and shear loadings are tabulated in figs. 16 to 19. Figs. 16 and 17 show the variation of G with δ_x^{tip} at various ψ for $r = 0$ and $r = 0.2$, respectively. Note that for $r = 0$ (i.e. minimal coupling) there is only a slight increase in δ_x^{tip} at instability as more tension is superposed. When $r = 0.2$, there is a more modest increase in δ_x^{tip} at instability with G. In cases where the G-δ_x^{tip} relation achieves zero slope before

$G = 2\gamma_s$, a dislocation is presumed to be emitted before tensile decohesion has a chance to become unstable. The emission criteria, expressed as plots of G_{disl} versus ψ, are shown in fig. 18. For comparison, the Rice-Thompson model, when expressed in terms of K_I and K_{II}, would give the result that emission on this uninclined slip plane is only dependent on K_{II}. Current results, however, show that tension across the slip plane decreases the amount of K_{II} needed to emit the dislocation. The effect of K_I becomes stronger as the dilation parameter r is increased. An "emission surface" [18] may be constructed in K_I-K_{II} space based on the G-ψ data, and is shown in fig. 19. The circle represents the Griffith criterion, the straight line is the K_{II} =constant result, and the curved lines represent current results. Because we have used a large value of q ($= \gamma_{us} / 2\gamma_s$) the ratio $\sqrt{q}$ of critical K_{II} (for pure mode II) to K_I (for pure mode I) is substantially higher than it would be for typical ductile metals.

Since the plots of G_{disl} versus ψ in fig. 18 are normalized such that G_{disl} is 1.0 at $\psi = 0°$, a comparison of the absolute values of G_{disl} given by the various methods is in order. A convenient way to make the comparison is to equate expressions for G_{disl} from both methods (at $\psi = 0°$), and then solve for r_c; this is the core cutoff parameter that would force the Rice-Thomson equation to give the newer result $G = \gamma_{us}$:

$$\frac{r_c}{b} = \frac{\cos^2\phi + (1-\nu)\sin^2\phi}{16\pi(1-\nu)}\left(\frac{\mu b}{\gamma_{us}}\right). \tag{30}$$

If it is assumed that γ_{us} lies in the range $\mu b/40$ to $\mu b/20$ as estimated based on [28] for Shockley partials in fcc crystals, then r_c/b should be about $0.6 - 1.2$. Recent evaluations of the Rice-Thomson equations for emission have often assumed $r_c / b = 1.0$ for simplicity [5], although other estimates exist (see [2] and references therein).

An important prediction retained by the new model is the moderate dependence on the phase angle. A boundary in a crystal could behave in a ductile *or* a brittle manner, depending on the mode of loading. Although the effect of slip plane inclination is not investigated in this work, the results there should not be surprising: certain orientations of the crystal should be favorable for dislocation emission, while others should be favorable for cleavage. Experiments on symmetric bicrystals of copper lend support to this claim [3,36]. Work is in progress to test dislocation nucleation ideas on metal/ceramic interfaces [36].

One implication of the dependence of dislocation emission on the slip-plane inclination angle is a cracking-*direction* dependence. A given interface containing at least one single crystal which shows a range of mechanical behaviour may behave in a brittle manner with a crack oriented to run in one direction, and may behave in a ductile fashion if the crack is oriented to run in the opposite direction (assuming that slip systems are oriented differently relative to the tip in the two cases). This kind of behaviour is observed in [3] and is discussed within the Rice-Thomson framework. In fcc crystals, not many interface planes strongly exhibit this type of behaviour due to the number of slip planes that are available for dislocations to move on. Some examples of planes which do show strong directional dependence in fcc are the {221} and {997} planes [3,36].

ACKNOWLEDGEMENTS

This research is supported by the NSF Materials Research Laboratory at Harvard (grant DMR-89-20490), the Office of Naval Research Mechanics Program (grant N00014-90-J-1379), and a University Research Initiative (subcontract POAVB38639-0 from the University of California, Santa Barbara, based on ONR/DARPA contract N00014-86-K-0753). Some of the computations were carried out under NSF support at the Pittsburgh Supercomputing Center. We are grateful to Y. Sun, I.-H. Lin and L. Truskinovsky for helpful discussion, and to Y. Huang for reviewing the manuscript.

REFERENCES

1. D. Mason, *Phil. Mag., 39* (1979), 455.

2. P. M. Anderson and J. R. Rice, *Scripta Met., 20* (1986), 1467.

3. J. S. Wang and P. M. Anderson, *Acta Met.*, in press.

4. J. R. Rice, in R. M. Latanision and R. H. Jones (eds.), *Chemistry and Physics of Fracture,* Martinus Nijhoff, Dordrecht, 1987, p. 22.

5. J. R. Rice, Z. Suo, and J. S. Wang, in M. Ruhle, A. G. Evans, M. F. Ashby, and J. P. Hirth (eds.), *Metal-Ceramic Interfaces,* Acta-Scripta Metallurgica Proceedings Series, Volume 4, Pergamon Press, 1990, pp. 269-294.

6. J. R. Rice and R. Thomson, *Phil. Mag., 15* (1974), 567.

7. S. J. Burns, *Scripta Met., 20* (1986), 1489.

8. G. Michot and A. George, *Scripta Met., 20* (1986), 1495.

9. S. M. Ohr, *Mat. Sci. and Engr., 72* (1985), 1.

10. Y.-H. Chiao and D. R. Clark, *Acta Met., 37* (1989), 203.

11. P. M. Anderson, Ph.D. Thesis, Harvard University, Cambridge, MA, U.S.A., 1986.

12. A. S. Argon, *Acta Met., 35* (1987), 185.

13. G. Schoeck, *Phil. Mag.*, in press.

14. J. R. Rice, manuscript in preparation.

15. J. R. Rice and J. S. Wang, *Mat. Sci. and Engr., A107* (1989), 23.

16. J. R. Rice, in H. Liebowitz (ed.), *Fracture: An Advanced Treatise,* vol. II, Academic Press, New York, 1968, p. 191.

17. J. R. Rice, *J. App. Mech., 35* (1968), 379.

18. R. Thomson, in H. Ehrenreich and D. Turnbull (eds.), *Solid State Physics*, vol. 39, Academic Press, New York, 1986, p. 1.

19. C. Hsieh and R. Thomson, *J. App. Phys., 44* (1973), 2051.

20. F. Prinz, H. O. K. Kirchner, and G. Schoeck, *Phil. Mag., 38* (1978), 321.

21. H. Gao and J. R. Rice, *J. Mech. Phys. Sol., 37* (1989), 155.

22. J. Yu and J. R. Rice, in M. H. Yoo, C. L. Briant, and W. A. T. Clark (eds.), *Interfacial Structure, Properties, and Design*, Materials Research Society, Vol. 122, 1988, p. 361.

23. P. M. Anderson, J. S. Wang, and J. R. Rice, in G. B. Olson, M. Azrin, and E. S. Wright (eds.), *Innovations in Ultrahigh-Strength Steel Technology*, Sagamore Army Materials Research Conference Proceedings, Vol. 34, 1990, p. 619.

24. R. E. Peierls, *Proc. Phys. Soc., 52* (1940), 23.

25. F. R. N. Nabarro, *Proc. Phys. Soc., 59* (1947), 59.

26. K. Cheung, Ph.D. Thesis, Massachusetts Institute of Technology, Cambridge, MA, U.S.A., 1990.

27. M. Yamaguchi, V. Vitek, and D. P. Pope, *Phil. Mag., 43* (1981), 1027.

28. Y. Sun, J. R. Rice, and L. Truskinovsky, manuscript in preparation.

29. J. H. Rose, J. R. Smith, and J. Ferrante, *Phys. Rev. B, 28* (1983), 1835.

30. J. H. Rose, J. R. Smith, F. Guinea, and J. Ferrante, *Phys. Rev. B, 29* (1984), 2963.

31. J. Ferrante and J. R. Smith, *Phys. Rev. B, 31* (1985), 3427.

32. A. Needleman, *J. Mech. Phys. Sol., 38* (1990), 289.

33. A. T. Paxton, P. Gumbsch, and M. Methfessel, submitted to *Physical Review Letters.*

34. H. Tada, P. C. Paris, and G. R. Irwin, *Stress Analysis of Cracks Handbook*, 2nd Ed., Del Research, 1985.

35. J. P. Hirth and J. Lothe, *Theory of Dislocations*, McGraw-Hill, New York, 1968.

36. J. S. Wang and G. E. Beltz, work in progress.

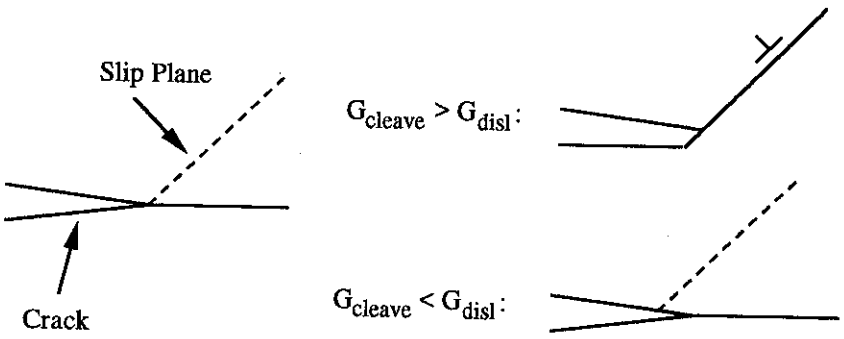

Figure 1. Atomistically sharp crack on the left, showing the competition between dislocation emission (upper right) and cleavage decohesion (lower right).

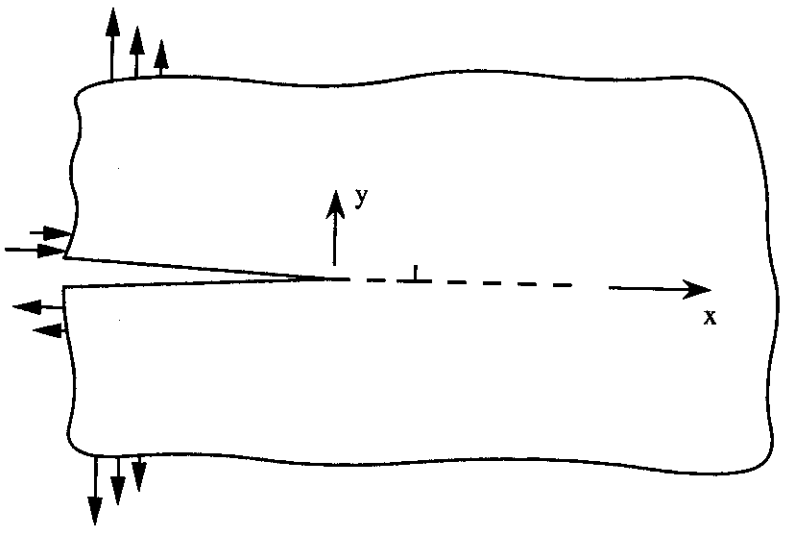

Figure 2. Geometry in 2-D for an emergent edge dislocation on a slip plane which is coplanar with the crack plane.

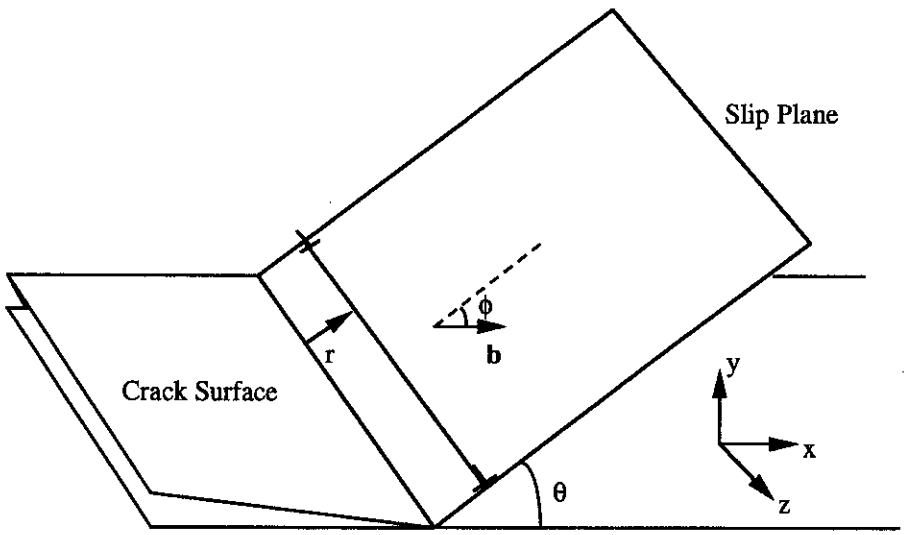

Figure 3. Geometry used in the Rice-Thomson analysis for the emission of a straight dislocation line.

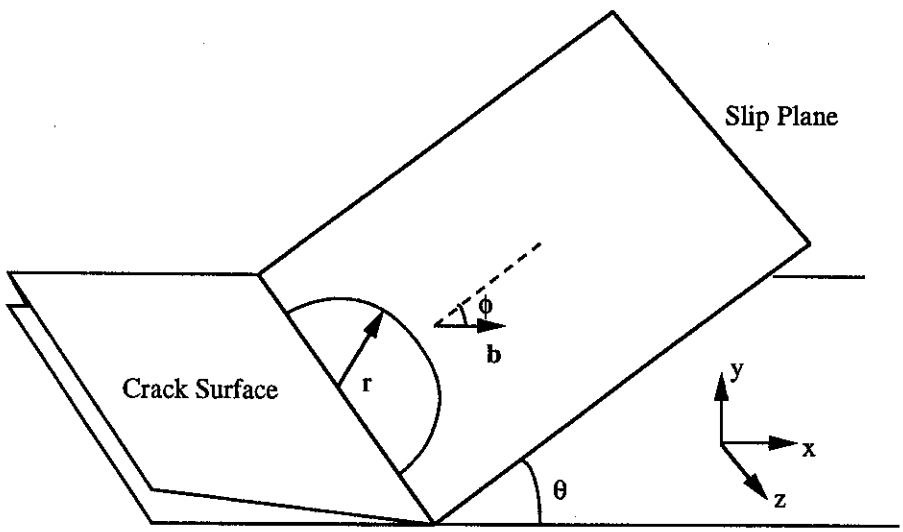

Figure 4. Geometry used in the Rice-Thomson analysis for an emergent semicircular dislocation loop.

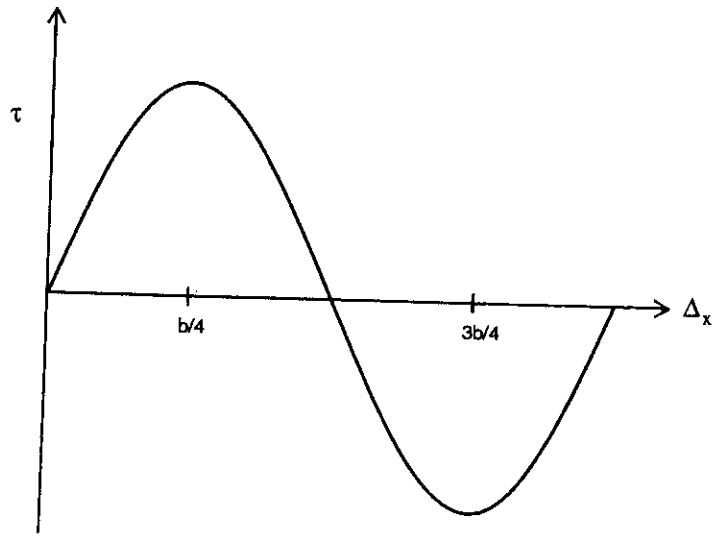

Figure 5. Expected form of the shear stress (τ) on a slip plane versus relative atomic displacement (Δ_x).

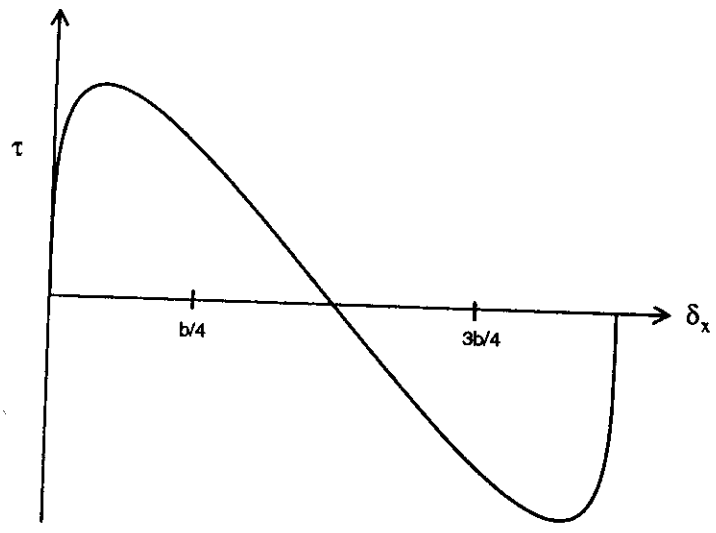

Figure 6. Expected form of the shear stress (τ) on a slip plane versus displacement discontinuity (δ_x).

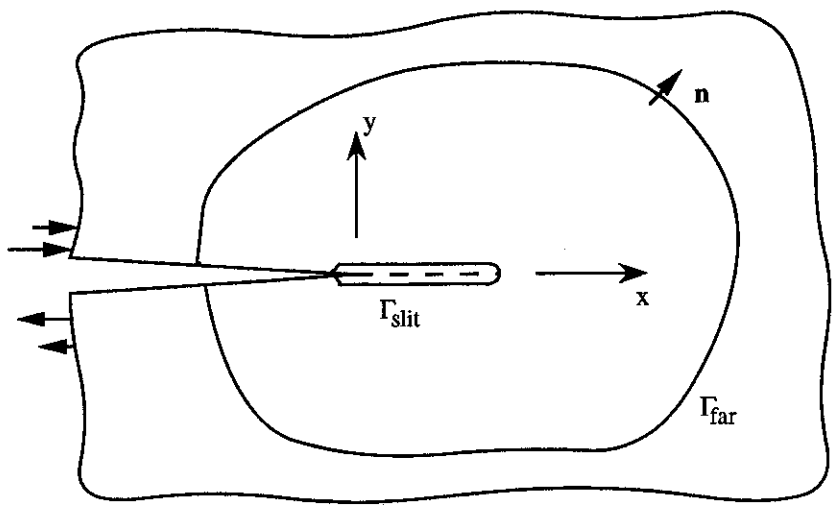

Figure 7. Geometry for evaluation of the J-integral on a path in the far field (Γ_{far}) and on a path which surrounds the slit which represents a slip plane (Γ_{slit}).

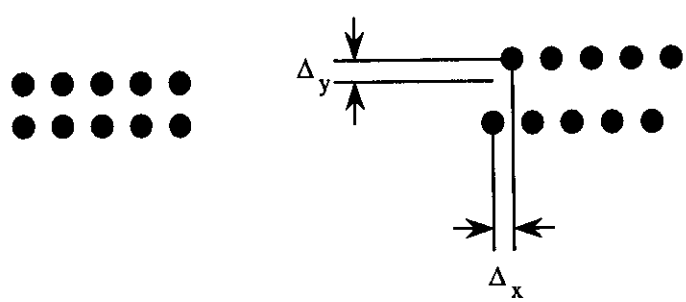

Figure 8. Schematic showing the combined relative atomic displacements in the x and y directions.

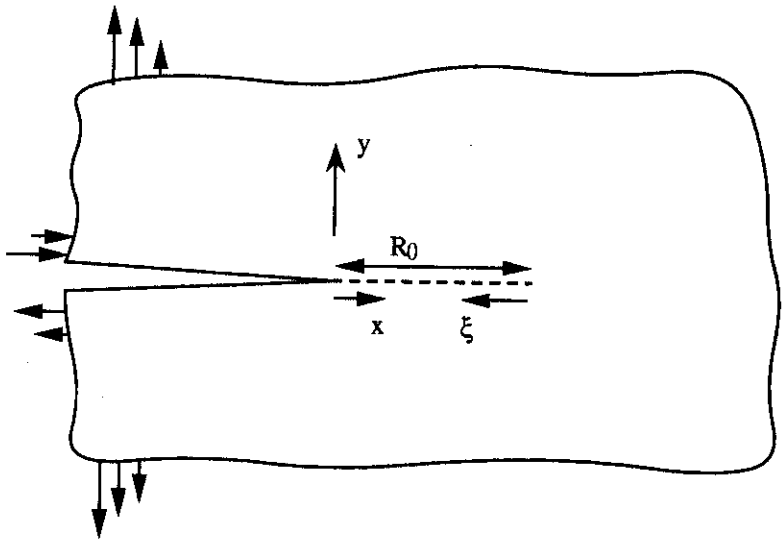

Figure 9. Coordinate frame used for setting up the integral equations which describe dislocation emission under a mixed-mode loading.

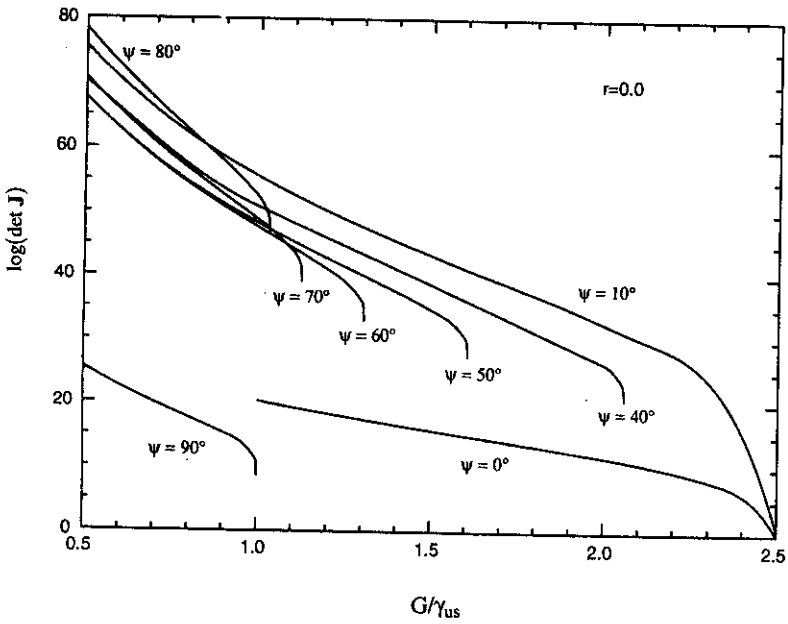

Figure 10. The variation of det **J** with applied energy release rate for various phase angles for r=0; note sharp decrease indicating the onset of instability.

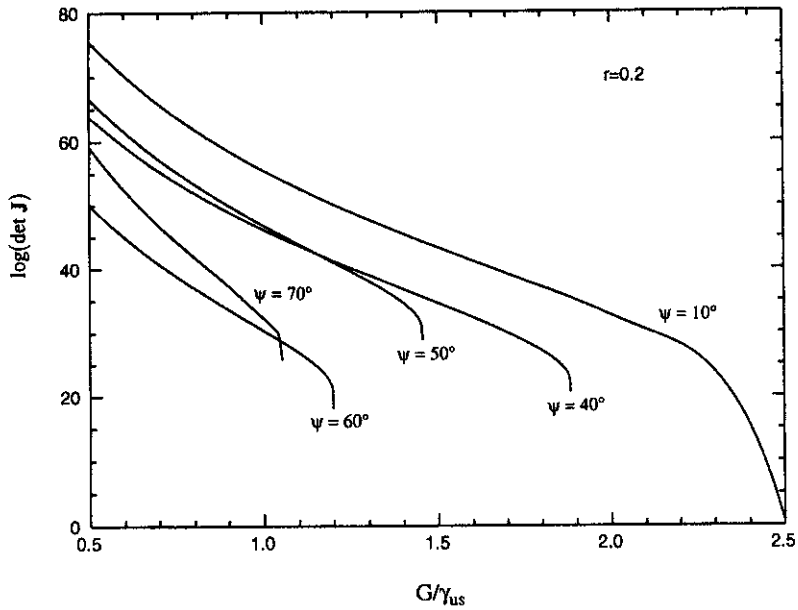

Figure 11. Variation of det J with applied energy release rate for r = 0.2.

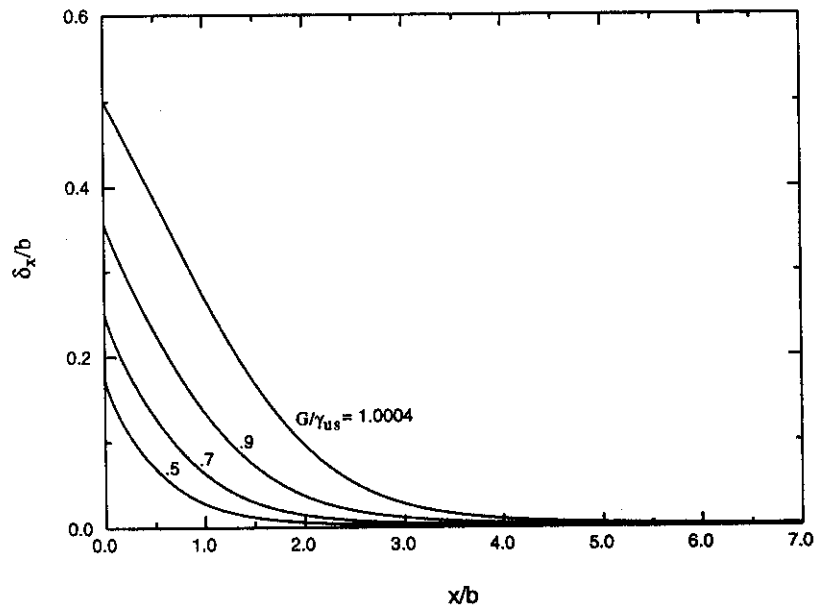

Figure 12. Displacement profiles at various levels of applied energy release rate up to instability for a pure mode II shear crack.

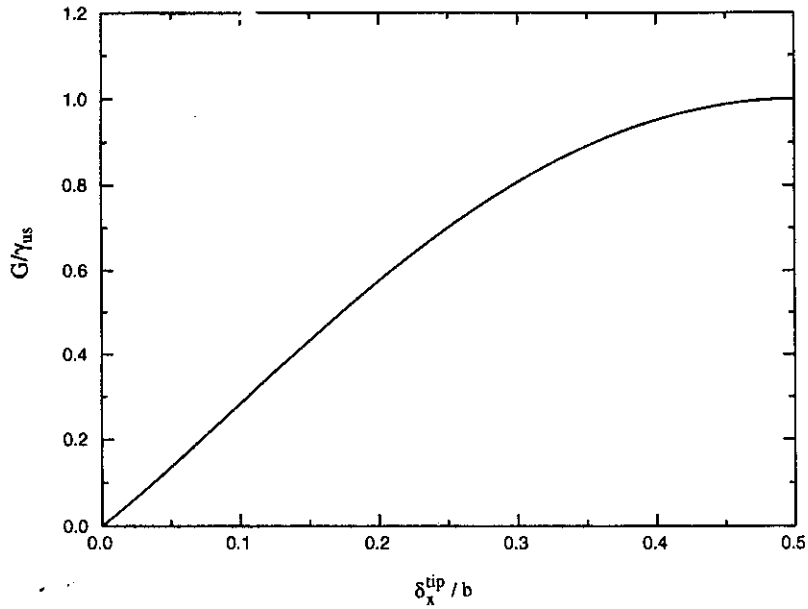

Figure 13. Applied energy release rate versus slip at the tip for a pure mode II shear crack.

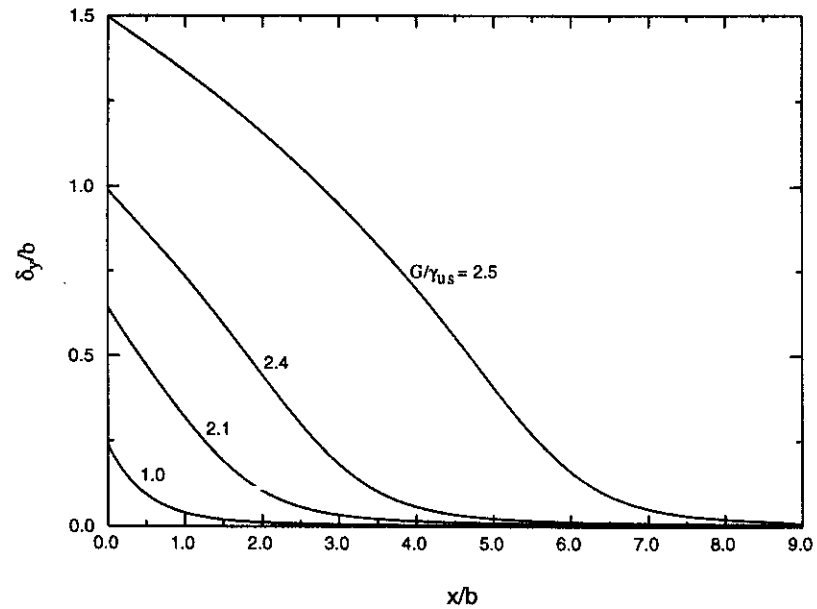

Figure 14. Opening profiles for various loadings up to instability for a mode I loading.

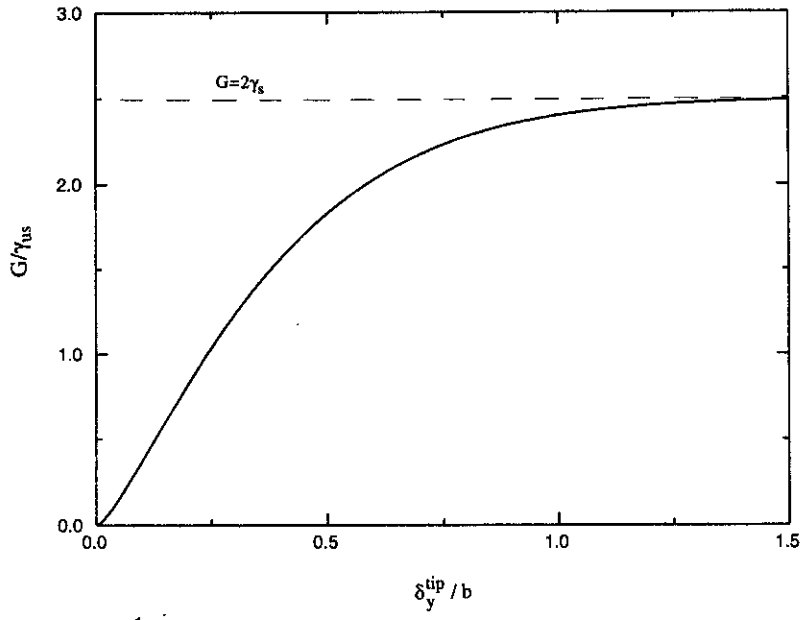

Figure 15. Applied energy release rate versus opening at the crack tip for a mode I loading.

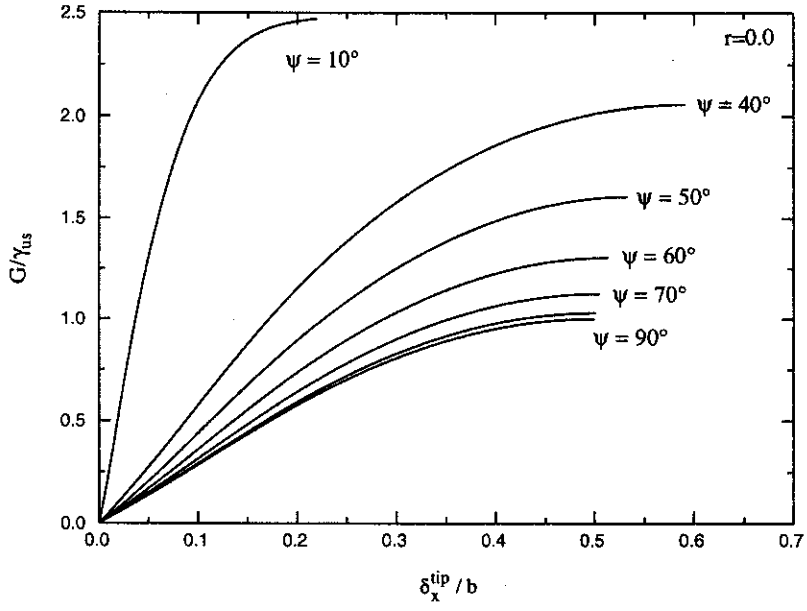

Figure 16. Applied energy release rate versus slip at the tip for various phase angles; r=0.

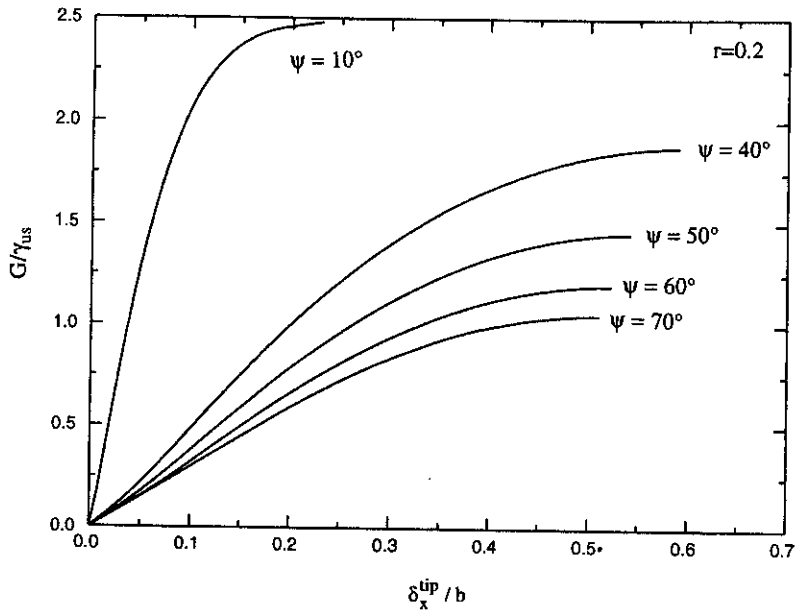

Figure 17. Applied energy release rate versus slip at the tip for various phase angles; r = 0.2.

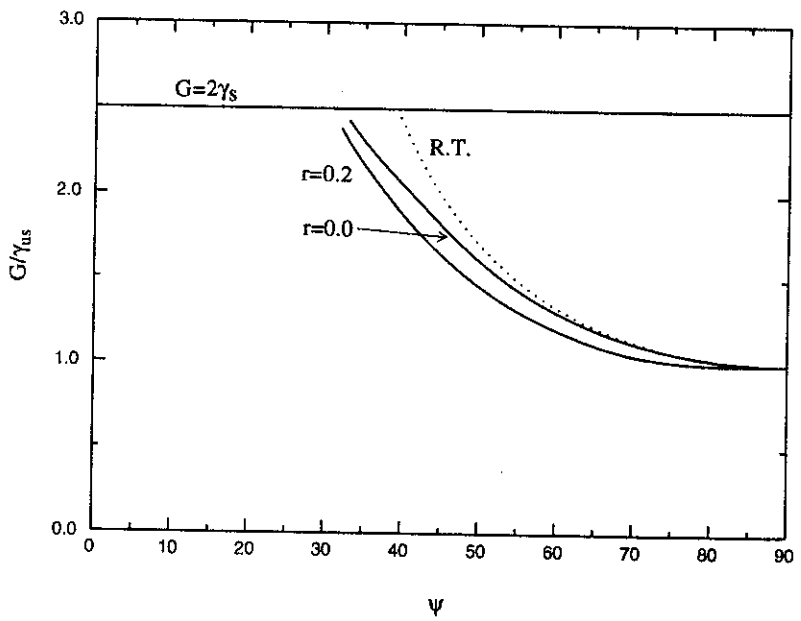

Figure 18. Critical G/γ_{us} for emission of a dislocation as a function of the phase angle for the two cases considered, r = 0 and 0.2, as well as the Rice-Thomson result.

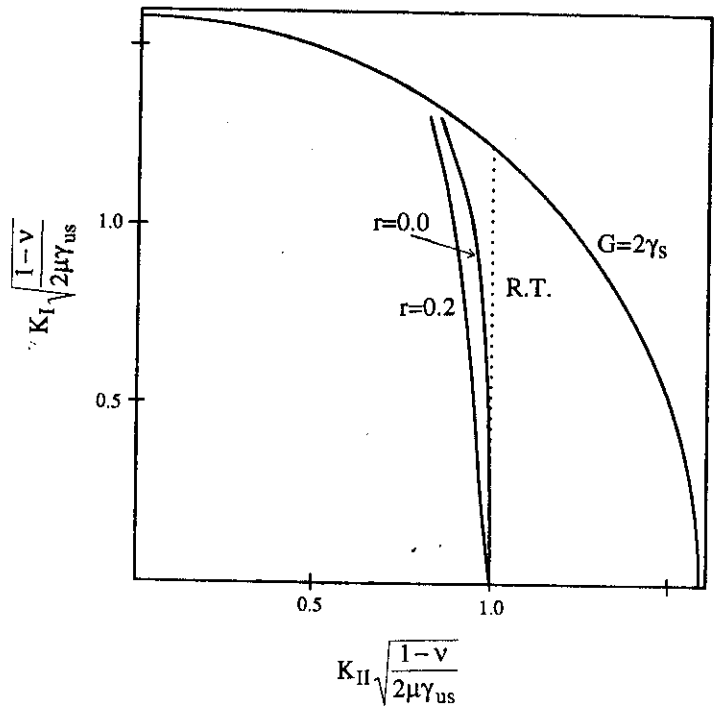

Figure 19. Emission surface based G-ψ data from fig. 18; the circle gives the Griffith condition for cleavage and the remaining curves give the emission condition.